



A method to determine the slip systems in BGA lead-free solder joints during thermal fatigue

Shihai Tan¹ · Jing Han¹ · Yan Wang¹ · Fu Guo¹

Received: 27 November 2017 / Accepted: 6 February 2018 / Published online: 15 February 2018
© Springer Science+Business Media, LLC, part of Springer Nature 2018

Abstract

The ball grid array (BGA) component with cross-sectioned edge row was thermally shocked to investigate the activated slip systems in the Sn–3.0Ag–0.5Cu lead-free solder joint. The microstructure and crystal orientations of Sn-based solder joints in as-reflowed and thermally shocked conditions were obtained by scanning electron microscopy (SEM) and electron back-scattered diffraction (EBSD), respectively. The sample was reexamined after 200, 300 and 400 thermal shock cycles without further polishing. In this paper, one single-crystal solder joint in a BGA component was selected to analyze the activated slip systems during recrystallization under the thermally shocked cycled condition. Two steps were used to determine the activated slip systems in this study. Step one, subgrain rotation angles and axes were calculated by the Euler angles obtained by EBSD before and after thermal shock. Then several slip systems were obtained according to the calculated subgrain rotation axes. Step two, in order to further determine the accurate slip system which could cause the subgrain rotation along the axes in step one, the theoretical slip traces were obtained by calculating Euler angles. Because the results contained many kinds of theoretical slip traces, so the slip bands observed by SEM were used and assisted to select the theoretical slip traces. Based on the comprehensive analysis of the two steps, slip systems that causes the serious deformation were determined. The results showed that recrystallization occurred at different areas of the solder joint and the slip bands appeared at the corners of the solder joint. The subgrain rotation behavior was variable at the recrystallization area by analyzing the subgrain orientation after 200, 300 and 400 thermal shock cycles. By compared the as-calculated slip traces with the slip bands characterized by SEM and the rotation axes calculated by the Euler angles, $(0\bar{1}0)[001]$, $(1\bar{1}0)[001]$ and $(110)[00\bar{1}]$ were the slip systems that caused the subgrain rotation along a certain axis in this solder joint.

1 Introduction

In the electronic information age, the density of electronic components increased with the Moore's law. The development of electronic packages trends to light-duty, miniaturization and multifunction, and the ball grid array (BGA) component plays an important role in the central processing unit of the large scale equipment (such as automotive, communications, aerospace and other fields) as the product of miniaturization and densification of electronic package. However, solder joints in the packages service under the high density of electronic condition where could generate

a lot of Joule Heat [1], so a serious issue was risen that recrystallization occurred under the thermal alternating environment caused by the switch on/off frequently [2, 3]. In recent years, researchers have done plenty of works to investigate recrystallization in the solder joints under the thermal cycling condition [4–9]. The results indicated that recrystallization occurred in the solder joints during thermal cycling, and the way to form recrystallized grains is subgrain rotation [10–13]. But there were also a few literatures which reported about the mechanism of recrystallization of lead-free solder joints in BGA components during thermal cycling. Thermal stress/strain exists in electronic packaging products during thermal cycling due to the mismatched coefficient of thermal expansion (CTE) [14]. So the recrystallized grains usually generate at the corners, the interface and the grain boundary of the solder joints due to the high-mismatched CTE [15]. Furthermore, the BGA component is a symmetrical structure and the stress induced by thermal cycling increased gradually from the center of the package

✉ Jing Han
hanjing@bjut.edu.cn

✉ Fu Guo
guofu@bjut.edu.cn

¹ College of Materials Science and Engineering, Beijing University of Technology, Beijing 100124, China

to corner. So, even if solder joints have the similar crystal orientation, the place where recrystallization occurred may not be identical with each other.

Accelerated thermal cycling is a common way to assess the reliability of solder joints under thermo-mechanical stress. And it has been widely reported in literatures that the primary failure mode in Sn-based solder joints is cracking near the package side during thermal cycling [16–18]. Several studies have been carried out to compare failure modes with real case, and these studies focused on the effect of different temperature profiles, grain size and different structure of the package [19–21]. Furthermore, the microstructure evolution and the crack propagation were observed in solder joints during thermal cycling [22–26]. The crystal orientation evolution which was caused by the subgrain rotation was identified as the mechanism of the recrystallization during thermal cycling, which the recrystallized region formed at the area of crystal orientation evolution and began to weaken in the solder joint. Meantime, cracks propagated along the recrystallized grain boundaries in the recrystallized regions until the solder joint failure [27]. Therefore, in order to improve the reliability of the solder joints, it was a great significance to research the mechanism of the recrystallization and the subgrain rotation behavior. Though there has been a lot of research on the continuous recrystallization, the mechanism of the recrystallization was not clear. In previous studies of the recrystallization, the researchers only focused on either the electron backscattered diffraction (EBSD) data or the scanning electron microscope (SEM) data and ignored the connection between the EBSD data and SEM data. In addition, the majority of the results were not accurate due to the process of further polishing which could change the (sub)grain orientations. Moreover, the grain orientation and microstructure evolution occurred simultaneously during recrystallization. So, it is necessary to research the mechanism of recrystallization by combining the grain orientation and microstructure.

In this paper, a single-crystal solder joint in the BGA component was selected to investigate the activated slip systems without polishing after 200, 300, 400 thermal shock cycles. Two steps were used to determine the activated slip systems during recrystallization. EBSD technique was used to obtain the grain orientations. The subgrain rotation axes and misorientation angles were obtained by calculated Euler angles. Then SEM technique was used to obtain the microstructure before and after thermal shock, and the slip bands were observed on the solder joint. Finally, the slip systems that caused the subgrain rotation along a certain axis were calculated and obtained by the two steps.

2 Experimental procedures

A BGA component was selected as the specimen with a 12 mm × 12 mm body size and a three-row perimeter array of 228 solder joints which had a 300 μm diameter and 500 μm pitch. The composition of the solder balls was Sn–3.0Ag–0.5Cu (wt%) (SAC305). Figure 1 showed the X-ray transmission image of the BGA component. The BGA component contained a 10 mm × 10 mm silicon die attached solder balls which were used to fit the silicon die and printed circuit board (PCB) together. The electrolytic Ni/Au surface finished on top of the Cu surface and the specimen was assembled onto a 2.0 mm thick Flame Retardant four (FR-4) PCB which had an organic surface preservative surface finish. A typical reflow profile about peak temperature of 245 °C was used to mount the BGA on the PCB and the dwell time was 1.5 min at temperature above 217 °C.

The outmost row of specimen was cross-sectioned, ground and polished prior to thermal shock, as shown in Fig. 2. The process of metallographic preparation was complied with the standard procedures. The outmost row was approximately across the center of solder joints. The colloidal silica suspension with 0.05 μm particle was used to the final polishing. Then the initial microstructure and grain orientation was observed using polarized light microscopy and scanning electron microscope (SEM, Quanta FEI 650) equipped with the electron backscattered diffraction (EBSD, Quanta FEI 650) system before thermal shock test. To protect the solder to oxidation and pollution, the specimen was placed in a vacuum quartz glass tube after EBSD characterization of each time. Finally,

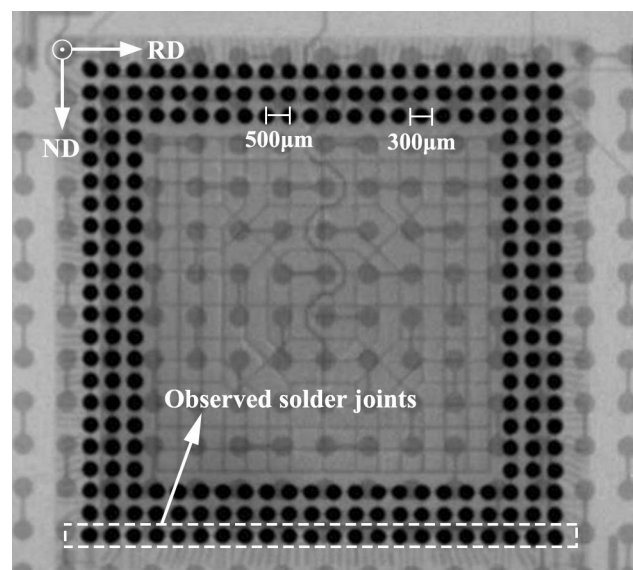


Fig. 1 X-ray transmission image of the BGA component

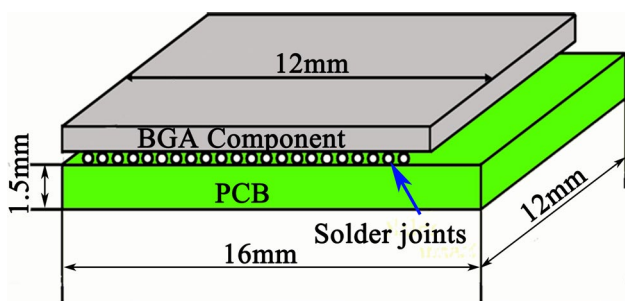


Fig. 2 Schematic of cross-sectioned BGA component for EBSD observation

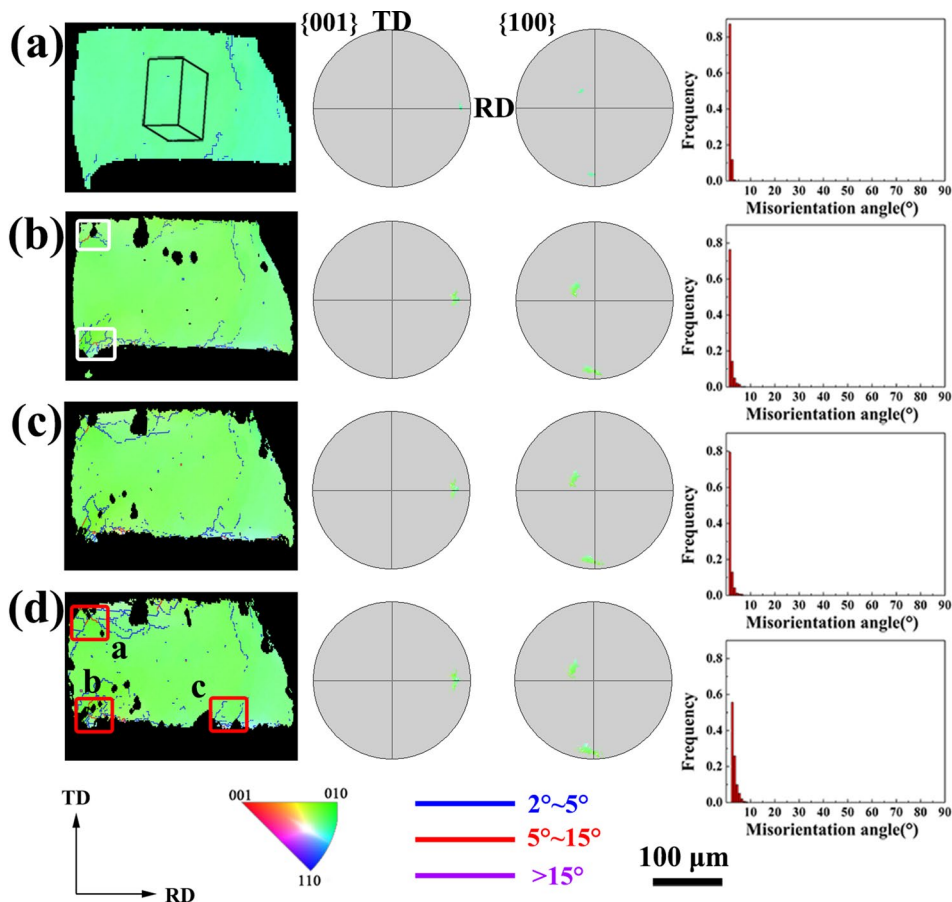
the specimen was placed in the thermal shock test furnace (BTS2-100B). The temperature profile of thermal shock was from -55 to 125 °C with 5 s cooling and heating ramp times and 15 min dwell times. After 200, 300 and 400 thermal shock cycles, the specimen was characterized again by EBSD and SEM without further polishing.

3 Results

Figure 3 showed the EBSD maps, $\{001\}$ and $\{100\}$ pole figures and misorientation angle distribution maps after 0, 200, 300 and 400 thermal shock cycles (named 0, 200, 300 and 400 TS, respectively). In the EBSD maps, the blue lines in the solder joint represented the low-angle grain boundaries, which were $> 2^\circ$ and $< 5^\circ$. The red lines in the solder joint represented the low-angle grain boundaries of 5° – 15° , and purple lines represented the high-angle grain boundaries.

Figure 3a shows the EBSD results before thermal shock, which indicated that the as-reflowed solder joint (0 TS) contains only a few low-angle grain boundaries and without high-angle grain boundaries. Then the solder joint could be considered as a single crystal solder joint in this study, which can be proved by $\{001\}$ and $\{100\}$ pole figures and the misorientation angle distribution map of 0 TS. The low-angle grain boundaries increased after 200 TS, and several subgrains were generated at the corners of the solder joint, as shown in the white rectangle frames in Fig. 3b. Moreover, pole figures show that the diffracted dots were scattered with the increased thermal

Fig. 3 EBSD maps, $\{100\}$ and $\{001\}$ pole figures and misorientation distribution maps, **a** 0 TS, **b** 200 TS, **c** 300 TS, **d** 400 TS. (Color figure online)



shock cycles. The misorientation angles and the range of the low-grain boundaries increased after 200 TS.

The EBSD results indicated that the grain orientation evolution occurred in the solder joint, and many subgrains were generated in the solder joint during thermal shock. With the increasing thermal shock cycles, many subgrains and subgrain boundaries were formed in the solder joint, as shown in Fig. 3c and d. The range of low-angle grain boundaries and misorientation angles increased gradually after 300 and 400 TS, and the pole figures show that the diffracted dots spread gradually around the initial diffracted dots. Furthermore, several dots in the pole figures were more scattered than that of the initial state, as shown in Fig. 3d. The results indicated that the grain orientations changed during thermal shock, and many subgrains formed in the solder joint.

In order to investigate the subgrain rotation behavior during thermal shock, the EBSD data was obtained without polishing after 200, 300 and 400 TS. Three areas (a, b and c) where subgrains formed at corners of the solder joint were selected to obtain the subgrain orientations after 200, 300 and 400 TS, as shown in the red rectangle frames of the Fig. 3d. In addition, the deformation occurred in the solder joint during thermal shock, and amounts of slip bands were characterized clearly after 300 TS, as shown in the red frames signed at areas a, b and c in Fig. 4c. The number of slip bands increased with the increasing number of thermal shock cycles. Figure 4e–g show the local magnified SEM maps of Fig. 4c at 300 TS. Three kinds of slip bands marked with colorful lines and numbers ①, ② and ③ were selected to analyze the slip systems.

4 Discussion

4.1 The analysis of slip directions using EBSD

The EBSD results were used to analyze the subgrain rotation behavior by calculating Euler angles. Figure 5 shows the grain orientations at areas a, b and c after 0, 200, 300 and 400 TS. The blue lines marked with angles that ranged from 2° to 5° represented the low-angle grain boundaries in the EBSD maps. The red lines represented the low-angle grain boundaries of 5° – 15° in the EBSD maps. The purple lines represented the high-angle grain boundaries. The frames marked with M, N and K represented the initial grain orientations which selected at areas a, b and c, respectively, as shown in Fig. 5a. The frames marked with A, B and C represented the grain orientations after 200 TS, as shown in Fig. 5b. The frames marked with D, E and F represented the grain orientations after 300 TS, as shown in Fig. 5c. The frames signed with G, H and I represented the grain orientations after 400 TS, as shown in Fig. 5d.

Because the subgrain orientations were obtained without further polishing after 200 TS, 300 TS and 400 TS, the EBSD data could be used to analyze the subgrain rotation behavior accurately. For example, at area a, the subgrain orientation A could be transformed from the initial orientation M after 200 TS. The subgrain orientation D could be transformed from the initial orientation M after 300 TS, whereas the subgrain orientation G could be transformed from the initial orientation M after 400 TS. At area b, the subgrain orientation B, E and H could be transformed from the initial orientation N after 200, 300 and 400 TS, respectively. At area c, the subgrain orientation C, F and I could

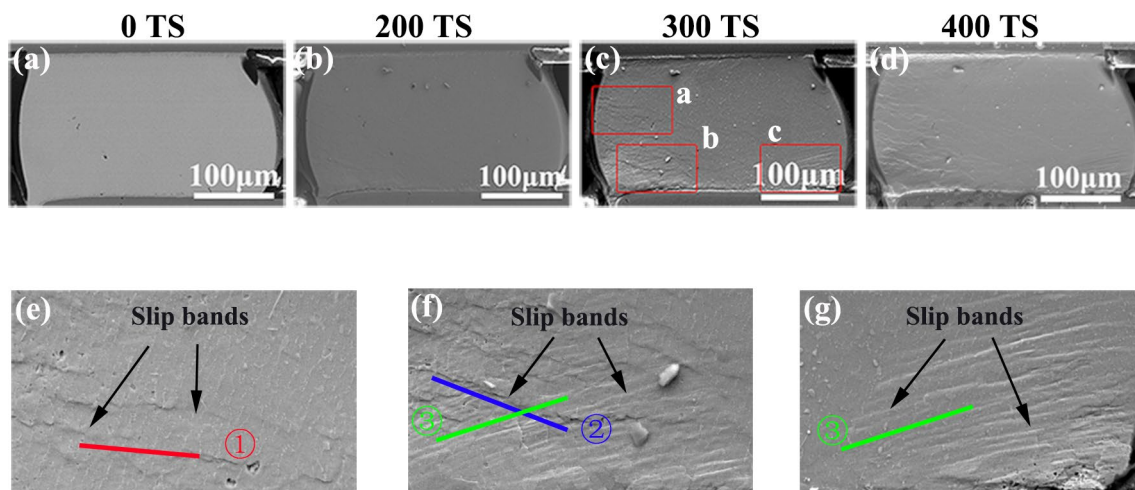
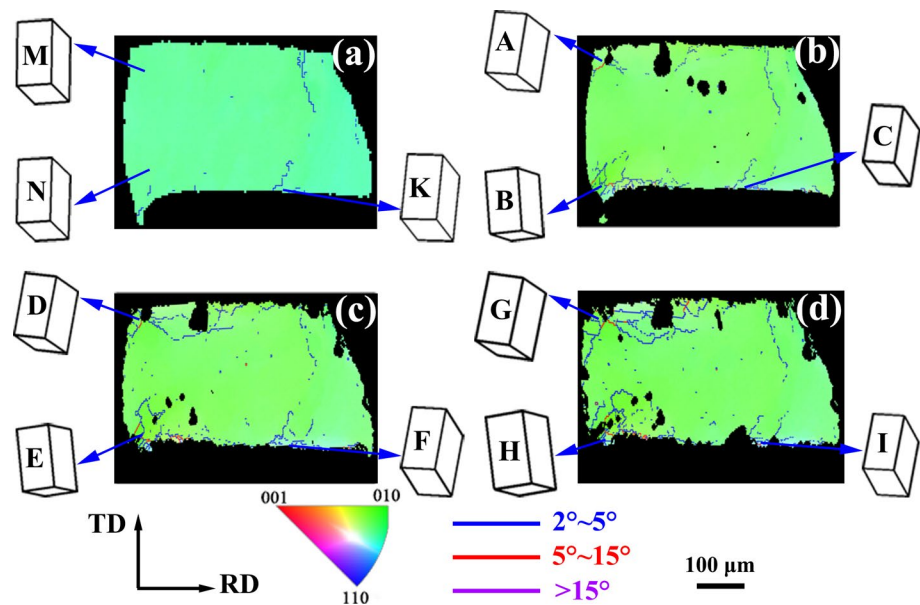


Fig. 4 SEM maps after **a** 0 TS, **b** 200 TS, **c** 300 TS and **d** 400 TS, respectively **e**, **f** and **g** magnified SEM maps of **c** at areas **a**, **b** and **c**, respectively

Fig. 5 (Sub)grain orientations at corners of the solder joint before and after thermal shock, **a** grain orientations *M*, *N* and *K* before thermal shock, **b** subgrain orientations *A*, *B* and *C* after 200 TS, **c** subgrain orientations *D*, *E* and *F* after 300 TS, **d** subgrains *G*, *H* and *I* after 400 TS. (Color figure online)



be transformed from the initial orientation *K* after 200, 300 and 400 TS, respectively.

Figure 6 showed the process of subgrain rotation analysis after 200, 300 and 400 TS by calculating Euler angles. The grain orientations were obtained by the EBSD data, which were correspond to the grain orientations in Fig. 5, and the black rectangle frame represented the initial orientation. The red, blue and pink rectangle frames represented the grain orientations after 200, 300 and 400 TS, respectively. For the area a, the grain rotation axes (RA) and the misorientation angles (MA) were $[\bar{1} 2 0]$ @ 10.0° , $[\bar{1} 2 1]$ @ 12.0° and $[\bar{1} 4 2]$ @ 13.2° after 200, 300 and 400 TS, respectively. For the area b, the grain rotation axes and the misorientation angles were $[\bar{3} 2 1 4]$ @ 10.5° , $[\bar{3} 2 1 1]$ @ 12.6° and $[\bar{2} 3 1 1]$ @ 12.4° after 200 TS, 300 and 400 TS, respectively. For the area c, the grain rotation axes and the misorientation angles were $[\bar{3} 2 8]$ @ 4.9° , $[1 2 \bar{7}]$ @ 6.4° and $[0 1 5]$ @ 7.9° after 200, 300 and 400 TS, respectively. The results indicate that the subgrain rotation axes and the misorientation angles were various at different areas of the solder joint during thermal shock. For area a, the rotation axes were close to Sn $[0 1 0]$, whereas the rotation axis was close to Sn $[0 0 1]$ at the areas b and c of the solder joint.

To the best of our knowledge, β -Sn is the body centered tetragonal structure with the length of $a_{[100]} = b_{[001]} \approx 2c_{[001]}$, so the axes $[1 0 0]$ and $[0 1 0]$ could be considered as the same rotation axis during analyzing the grain rotation behavior due to the symmetrical feature. As reported in the literature, there are fifteen common nonequivalent slip systems in Sn, and the slip system with the lowest ideal shear resistance is $(1 0 1) [\bar{1} 0 1]$ [28]. The literature reported that the subgrain rotation axes were likely the slip directions [8]. So, for area a, the activated slip system groups $(1 0 0) [0 1 0]$, $(0$

$0 1) [1 0 0]$ and $(1 0 1) [0 1 0]$ could cause the initial grain orientation *M* rotate along Sn $[1 0 0]$ into the grain orientations *A*, *D* and *G* after 200, 300 and 400 TS. For areas b and c, the activated slip system groups $(1 0 0) [0 0 1]$ and $(1 1 0) [0 0 1]$ could cause the initial grain orientation *N* (*K*) rotate along Sn $[0 0 1]$ into the grain orientations *B* (*C*), *E* (*F*) and *H* (*I*) after 200, 300 and 400 TS. However, the activated slip systems depended on the grain orientation and the stress direction.

Figure 7 showed the misorientation angles at different areas with the increasing thermal shock cycles. The lines signed with *A*, *B* and *C* represented the smallest misorientation angle of areas a, b and c after 200, 300 and 400 TS. For areas a and b, the misorientation angles increased after 300 and 400 TS, but the growth ratio decreased. Whereas, for the area c, the misorientation angle increased after 300 and 400 TS and the growth ratio increased. The results indicated that the misorientation angle increased with the increasing thermal shock cycles, but the growth ratio was invariable at different areas of the solder joint. The main reason caused the phenomenon was closely related to the cyclic thermal stress, which could cause different groups of slip systems activate during thermal shock.

4.2 The analysis of slip plane using SEM

The results of Fig. 6 showed that the subgrain rotation behavior (rotation axes and rotation angles) at areas a, b and c was different between each other, though the initial state of grain orientation was similar, which meant that the joint selected in this paper was the single crystal structure, as analyzed in Chap. 3.1. Then the results demonstrated that there could not be only one slip system activated in the

Fig. 6 Subgrain rotation analysis at areas a, b and c after 200, 300 and 400 TS, respectively

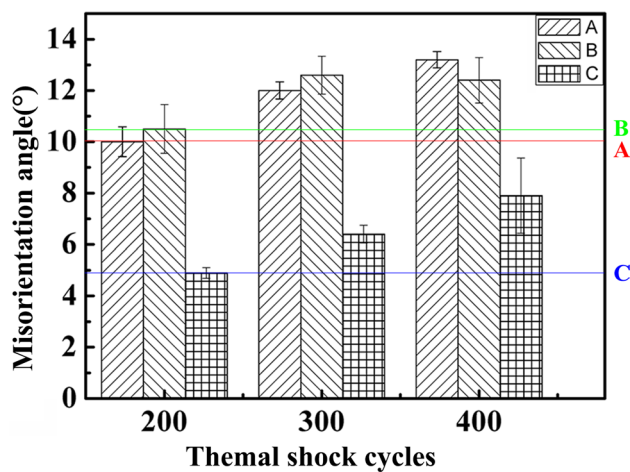
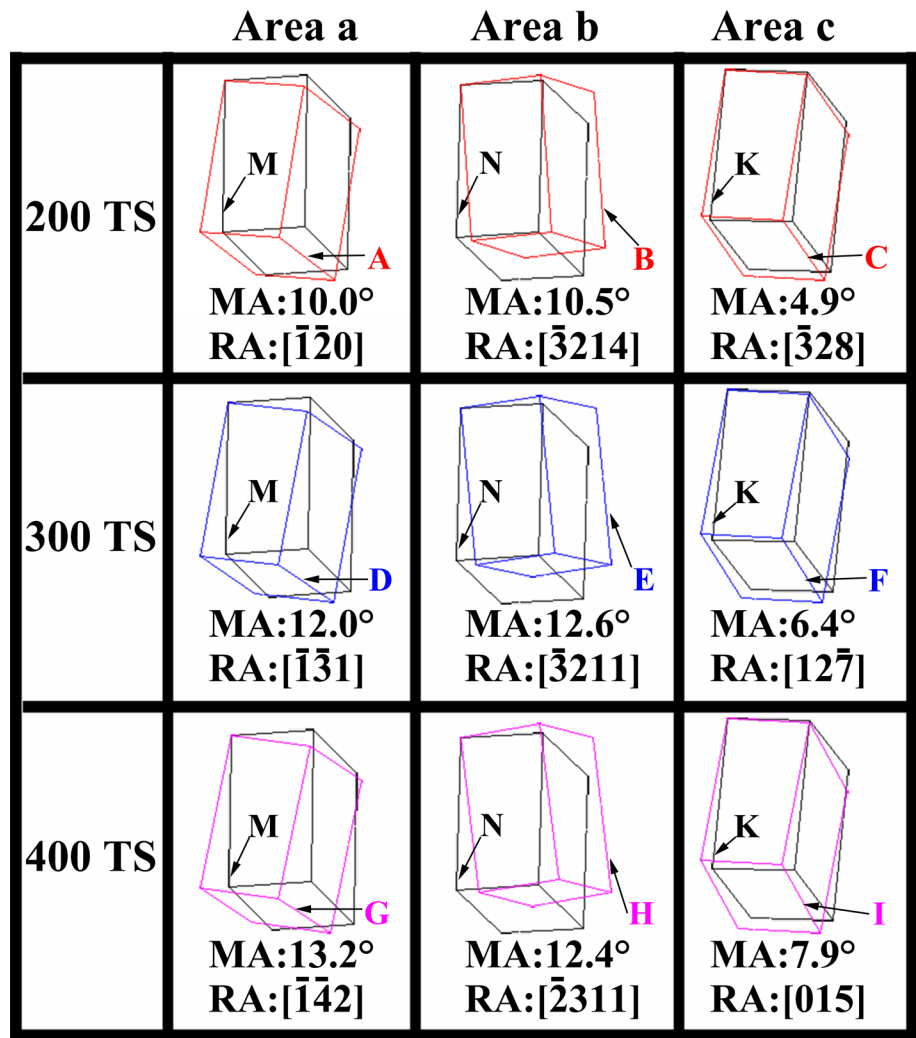
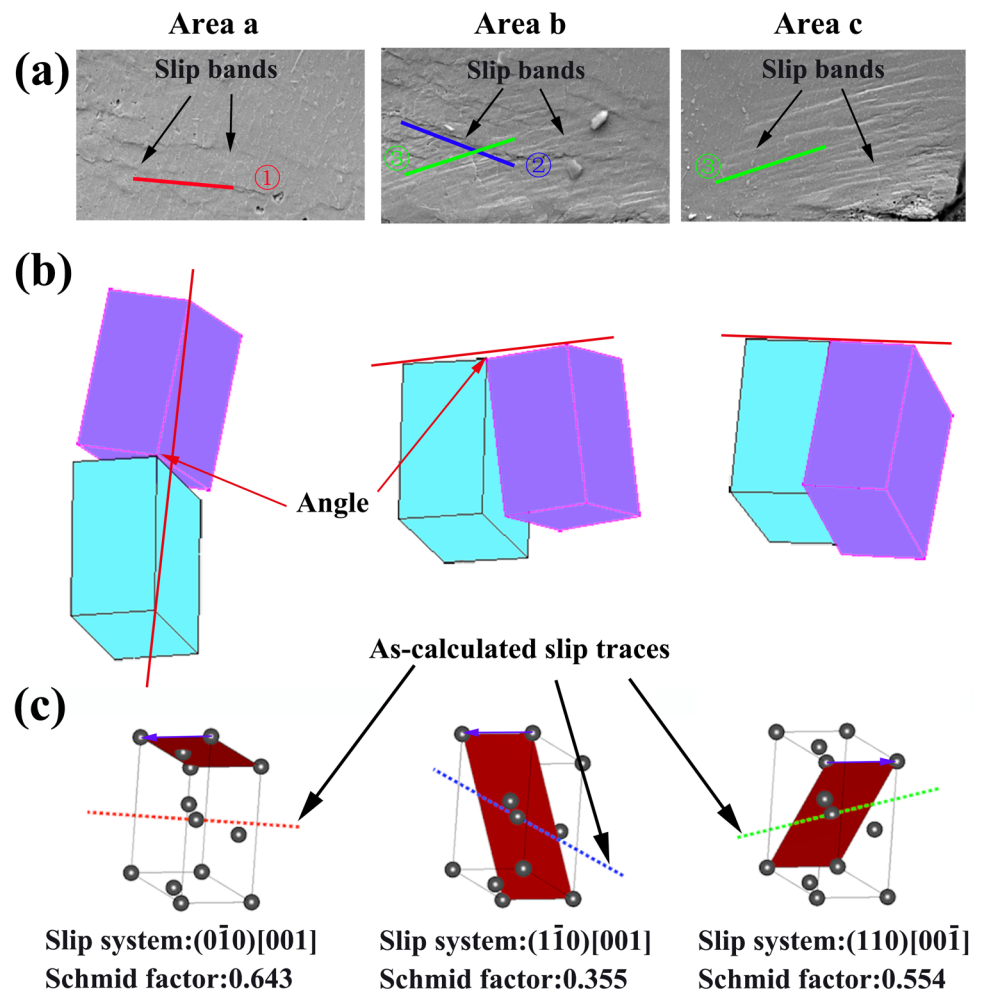


Fig. 7 The analysis of misorientation angle at areas a, b and c after 200, 300 and 400 TS, respectively. The colorful lines with A, B and C represent the minimum value of the misorientation angle

solder joint, and the stress was non-uniform distribution in the solder joint. Therefore, in order to determine a certain slip system that could cause the subgrain rotate about Sn [1 0 0] and [0 0 1], another step was used to determine the accurate slip systems by using SEM results. Many slip bands could be observed on the solder joint after 300 TS, as shown in Fig. 8a.

The generalized Schmid Factors (SF) for each given slip system were calculated with the Euler angles and listed in Table 1 (SF > 0.3) [29, 30]. The theoretical calculated slip traces are obtained with the theoretical calculated Schmid Factors. However, only three slip systems with theoretical calculated slip traces could match the slip bands in SEM maps, as shown in Fig. 8(c). For the slip bands ⊕, (0 1 0) [0 0 $\bar{1}$] is the slip system that could be activated with the short burgers factor and high SF (0.643). For the slip bands ⊗, (1 1 0) [0 0 $\bar{1}$] is the theoretical calculated slip system with blue slip trace that could be activated during thermal shock. For the slip bands ⊙, (1 $\bar{1}$ 0) [0 0 1] is the theoretical calculated slip system with green slip trace that

Fig. 8 **a** Magnified SEM maps of Fig. 4a at areas a, b and c, respectively **b** subgrain rotation behaviors at areas a, b and c slip systems with as-calculated slip traces that can match the slip bands characterized by SEM



could be activated during thermal shock. The results show that slip systems $(0\bar{1}0)[001]$, $(1\bar{1}0)[001]$ and $(110)[00\bar{1}]$ contained in the slip system groups $(100)[001]$ and $(110)[001]$. So $(0\bar{1}0)[001]$, $(1\bar{1}0)[001]$ and $(110)[00\bar{1}]$ were the slip systems that activated in the solder joint during thermal shock, and the rotation axes may be the slip direction.

However, from the results above, at area b, the activated slip systems were $(110)[00\bar{1}]$ and $(1\bar{1}0)[001]$, which were contained in the slip groups $(110)[001]$ that was obtained by the rotation axis $[001]$. At area c, the activated slip system was $(1\bar{1}0)[001]$, which were also contained in the slip groups $(110)[001]$ that was obtained by the rotation axis $[001]$. While $(010)[00\bar{1}]$ that was the activated slip system at area a was not contained in anyone slip groups $(100)[001]$, $(001)[100]$ and $(101)[010]$ obtained by the rotation axis $[100]$. The results indicated that the activated slip system at area a was not determined by this method. The main reason may be caused by the tolerance that was introduced by the calculating rotation axes and the relationship between rotation axes and slip directions. Then the method need to be further investigated.

The results showed that though the solder joint was the single crystal solder joint, several slip systems could be activated in the solder joint of the BGA components. The main reason may be caused by the stress distributed unevenly, and the stress at areas a and b was much larger than that at area c, leading to the difference of the misorientation angles at areas a, b and c, as shown in Fig. 7. The misorientation angles at areas a and b were much larger than that at area c. Furthermore, the SEM results showed that there were a lot of curved slip bands at areas a and b, as shown in Fig. 8a, which could prove that there were not only one slip system activated during thermal shock, while there were mounts of smooth slip bands at area c, then one slip system was activated. Figure 8b showed that subgrain rotation behavior at areas a and b was much more complicated than that at area c. Because the rotation axes in two grain orientation before and after thermal shock were not on a straight line and there was an angle, while the rotation axes of the grain orientations were ranged in a line at area c. The result indicated that more than one slip system was activated at areas a or b. So, in this study, several slip systems could be activated in one single crystal solder joint at different areas, and there was

Table 1 Schmid factors of the solder joint

Plane	Direction	SF
(1 0 $\bar{1}$)	[0 1 0]	0.678
(0 1 0)	[0 0 $\bar{1}$]	0.643
(0 0 1)	[0 $\bar{1}$ 0]	0.643
(1 $\bar{1}$ 0)	[0 0 1]	0.554
(0 0 1)	[1 $\bar{1}$ 0]	0.554
(1 0 $\bar{1}$)	$[\bar{1}$ 1 $\bar{1}$]/2	0.545
(0 1 0)	[1 0 $\bar{1}$]	0.516
($\bar{2}$ $\bar{1}$ 1)	[1 $\bar{1}$ 1]	0.503
($\bar{2}$ $\bar{1}$ 1)	[0 $\bar{1}$ $\bar{1}$]	0.465
(1 0 1)	[0 $\bar{1}$ 0]	0.451
(0 1 1)	[1 $\bar{1}$ 1]/2	0.394
(0 1 $\bar{1}$)	[0 1 1]	0.373
(1 2 1)	[1 0 $\bar{1}$]	0.373
(1 1 0)	[0 0 $\bar{1}$]	0.355
(0 0 1)	$[\bar{1}$ $\bar{1}$ 0]	0.355
(1 0 $\bar{1}$)	[1 1 1]/2	0.35
(2 $\bar{1}$ 1)	$[\bar{1}$ $\bar{1}$ 1]/2	0.347
(1 $\bar{2}$ 1)	$[\bar{1}$ 0 1]	0.341
($\bar{2}$ 1 1)	[0 $\bar{1}$ 1]	0.326
(0 1 1)	[0 $\bar{1}$ 1]	0.316
(1 0 1)	[1 $\bar{1}$ $\bar{1}$]/2	0.314
($\bar{2}$ 1 1)	$[\bar{1}$ $\bar{1}$ 1]/2	0.303

more than one slip system activated at the same area of the solder joint during thermal shock.

5 Conclusion

In this study, two steps were used to analyze the subgrain rotation behavior in a single crystal solder joint of the BGA component. The data was obtained by the EBSD technique without further polishing after 200, 300 and 400 TS, and the activated slip systems could be determined during deformation under the thermal shock cycles condition. By analyzing the subgrain rotation behavior, [0 1 0] and [0 0 1] seem to be the rotation axes with different misorientation angles. The misorientation angle increased with the increasing number of thermal shock cycles. The results of SEM show that a lot of slip bands appeared at the corners of the solder joint after thermal shock cycles, and Schmid factors and several as-calculated slip traces were obtained by calculated the Euler angles to determine the activated slip system. By the two steps analysis, (0 $\bar{1}$ 0) [0 0 1], (1 $\bar{1}$ 0) [0 0 1] and (1 1 0) [0 0 $\bar{1}$] were determined as the slip systems that activated in the solder joint during thermal shock cycles and the rotation axes may be the slip directions. The results also show that several slip systems could be activated at different areas of the single crystal solder joint, and more than one slip system

could be activated at the same area of the solder joint. The misorientation angles at areas with multiple slip systems is much larger than that at area with the single slip system. In the future, the slip systems that were activated during thermal shock will be investigated and analyzed by transmission electron microscope to better understand the process of recrystallization in the lead free solder joints.

Acknowledgements The authors acknowledge the support of this work from National Natural Science Foundation of China (No. 51401006), Beijing Natural Science Foundation (Nos. 2162005 and 2172009) and the Science and Technology Project of Beijing Municipal Education Commission (No. KM201710005003).

References

1. J.Q. Chen, J.D. Guo, K.L. Liu, J.K. Shang, Dependence of electromigration damage on Sn grain orientation in Sn-Ag-Cu solder joints. *J. Appl. Phys.* **114**, 153509 (2013)
2. H.T. Ma, W.D. Xie, G. Subbarayan, Effects of multiple reworks on the accelerated thermal cycling and shock performance of lead-free BGA assemblies. *IEEE Trans. Comp. Packag. Manuf.* **2**, 1824–1831 (2012)
3. J. Sitek, M. Koscielski, K. Bukat, M. Jakubowska, W. Niedzwiedz, A. Mlozniak, Influence of silver nanopowders addition to the SAC solder paste on thermal and mechanical fatigue properties of solder joints. *Prz. Elektrotechniczn.* **88**, 79–82 (2012)
4. A. Qasaimeh, S. Hamasha, Y. Jaradat, P. Borgesen, Damage evolution in lead free solder joints in isothermal fatigue. *J. Electron. Packag.* **137**, 021012 (2015)
5. A. Shirazi, H. Lu, A. Varvani-Farahani, Fatigue behaviour of lead-free solder interconnections in life prediction of trilayer structures subjected to thermal cycling. in *Proceedings of the Asme 10th International Manufacturing Science and Engineering Conference*, vol 1 (2015)
6. K.C. Wu, S.Y. Lin, T.Y. Hung, K.N. Chiang, Reliability assessment of packaging solder joints under different thermal cycle loading rates. *IEEE Trans. Device Mater. Reliab.* **15**, 437–442 (2015)
7. Q. Zhou, B.T. Zhou, T.K. Lee, T. Bieler, Microstructural evolution of SAC305 solder joints in wafer level chip-scale packaging (WLCSPP) with continuous and interrupted accelerated thermal cycling. *J. Electron. Mater.* **45**, 3013–3024 (2016)
8. J. Han, F. Guo, J.P. Liu, Early stages of localized recrystallization in Pb-free BGA solder joints subjected to thermomechanical stress. *J. Alloy. Compd.* **704**, 574–584 (2017)
9. J. Han, F. Guo, J.P. Liu, Effects of anisotropy of tin on grain orientation evolution in Pb-free solder joints under thermomechanical stress. *J. Mater. Sci.-Mater. Electron.* **28**, 6572–6582 (2017)
10. B.T. Zhou, G. Muralidharan, K. Kurumadalli, C.M. Parish, S. Leslie, T.R. Bieler, Microstructure and Sn crystal orientation evolution in Sn-3.5Ag lead-free solders in high-temperature packaging applications. *J. Electron. Mater.* **43**, 57–68 (2014)
11. J. Han, S. Tan, F. Guo, Study on subgrain rotation behavior at different interfaces of a solder joint during thermal shock. *J. Electron. Mater.* **45**, 6086–6094 (2016)
12. S. Tan, J. Han, F. Guo, Subgrain rotation at twin grain boundaries of a lead-free solder joint during thermal shock. *J. Mater. Sci.-Mater. Electron.* **27**, 9642–9649 (2016)
13. F.G.J. Han, J.P. Liu, Recrystallization induced by subgrain rotation in Pb-free BGA solder joints under thermomechanical stress. *J. Alloy. Compd.* **698**, 706–713 (2017)

14. M.A. Matin, W.P. Vellinga, M.G.D. Geers, Thermomechanical fatigue damage evolution in SAC solder joints. *Mater. Sci. Eng. A* **445**, 73–85 (2007)
15. T.R. Bieler, H.R. Jiang, L.P. Lehman, T. Kirkpatrick, E.J. Cotts, B. Nandagopal, Influence of Sn grain size and orientation on the thermomechanical response and reliability of Pb-free solder joints. *IEEE Trans. Comp. Packag. Technol.* **31**, 370–381 (2008)
16. P.E. Tegehall, G. Wetter, Impact of laminate cracks under solder pads on the fatigue lives of ball grid array solder joints. *Microelectron. Reliab.* **55**, 2354–2370 (2015)
17. X. Xu, G.Q. Chen, M.S. Cheng, Study on the failure behavior of BGA solder interconnections under fatigue loading. in 2015 16th International Conference on Electronic Packaging Technology (2015)
18. T. Garami, O. Krammer, G. Harsanyi, P. Martinek, Method for validating CT length measurement of cracks inside solder joints. *Solder. Surf. Mt. Technol.* **28**, 13–17 (2016)
19. S. Terashima, M. Tanaka, K. Tatsumi, Thermal fatigue properties and grain boundary character distribution in Sn-xAg-0.5Cu ($x = 1, 1.2$ and 3) lead free solder interconnects. *Sci. Technol. Weld. Join.* **13**, 60–65 (2008)
20. J. Hokka, T.T. Mattila, H.B. Xu, M. Paulasto-Krockel, Thermal cycling reliability of Sn-Ag-Cu solder interconnections-part 2: failure mechanisms. *J. Electron. Mater.* **42**, 963–972 (2013)
21. J. Hokka, T.T. Mattila, H.B. Xu, M. Paulasto-Krockel, Thermal cycling reliability of Sn-Ag-Cu solder interconnections: part 1: effects of test parameters. *J. Electron. Mater.* **42**, 1171–1183 (2013)
22. J.T. Liu, Z.G. Wang, J.K. Shang, Deformation behaviors of [110] and [112] oriented beta-Sn single crystals. *Acta Metall. Sin.* **44**, 1409–1414 (2008)
23. M. Berthou, P. Retailleau, H. Fremont, A. Guedon-Gracia, C. Jephos-Davennel, Microstructure evolution observation for SAC solder joint: comparison between thermal cycling and thermal storage. *Microelectron. Reliab.* **49**, 1267–1272 (2009)
24. T.K. Lee, K.C. Liu, T.R. Bieler, Microstructure and orientation evolution of the Sn phase as a function of position in ball grid arrays in Sn-Ag-Cu solder joints. *J. Electron. Mater.* **38**, 2685–2693 (2009)
25. P.J. Shang, Z.Q. Liu, D.X. Li, J.K. Shang, Crack propagation of single crystal beta-Sn during in situ TEM straining. *J Electron Microsc.* **59**, S61–S66 (2010)
26. B.T. Zhou, T.R. Bieler, T.K. Lee, K.C. Liu, Crack development in a low-stress PBGA package due to continuous recrystallization leading to formation of orientations with [001] parallel to the interface. *J. Electron. Mater.* **39**, 2669–2679 (2010)
27. L. Yin, L. Wentlent, L.L. Yang, B. Arfaei, A. Oasaimah, P. Borgesen, Recrystallization and precipitate coarsening in Pb-free solder joints during thermomechanical fatigue. *J. Electron. Mater.* **41**, 241–252 (2012)
28. Y. Kinoshita, H. Matsushima, N. Ohno, Predicting active slip systems in beta-Sn from ideal shear resistance. *Model. Simul. Mater. Sci. Eng.* **20**, 035003 (2012)
29. B.T. Zhou, Q. Zhou, T.R. Bieler, T.K. Lee, Slip, crystal orientation, and damage evolution during thermal cycling in high-strain wafer-level chip-scale packages. *J. Electron. Mater.* **44**, 895–908 (2015)
30. P. Darbandi, T.K. Lee, T.R. Bieler, F. Pourboghra, Crystal plasticity finite element study of deformation behavior in commonly observed microstructures in lead free solder joints. *Comput. Mater. Sci.* **85**, 236–243 (2014)